ChemComm
Chemical Communications

Accepted Manuscript

This article can be cited before page numbers have been issued, to do this please use: N. Zhao, C. Ma, W. Yang, W. Yin, J. Wei and N. Li, *Chem. Commun.*, 2019, DOI: 10.1039/C9CC04041B.

ROYAL SOCIETY OF CHEMISTRY

rsc.li/chemcomm

View Article Online
DOI: 10.1039/C9CC04041B

COMMUNICATION

Facile construction of boranil complexes with aggregation-induced emission characteristics and their specific lipid droplets imaging applications

Received 00th January 20xx,
Accepted 00th January 20xx

DOI: 10.1039/x0xx00000x

Na Zhao,*[a] Chengcheng Ma,[a†] Weiyao Yang,[a†] Wei Yin,[a] Jiahui Wei[a] and Nan Li*[a]

A rational strategy was reported to construct boranil complexes (DPFB derivatives) with unique aggregation-induced emission effect by installing phenyl rings in anil ligand as the intramolecular rotors. In view of the good biocompatibility and suitable lipophilicity, DPFB derivatives can serve as the excellent fluorescent probes for specific imaging of lipid droplets in living cells and yolk lipids in zebrafish.

Boron complexes based fluorescent materials have received considerable attentions due to their potential applications in the field of photoelectric devices, information storage elements, fluorescent sensors and probes.[1-2] However, some conventional boron complexes, such as difluoroboron dipyrromethene (BODIPY), suffer from the aggregation-caused quenching (ACQ) effect because of its coplanar conformation and intrinsic intermolecular π–π stacking.[3] The ACQ phenomenon limited the practical applications of boron complexes in solid devices or biological environment. Fortunately, an opposite phenomenon termed aggregation-induced emission (AIE) was discovered by Tang's group in 2001.[4] The AIE luminogens (AIEgens) exhibit faint emission in molecular dissolved state, but give enhanced emission in the aggregated state with the mechanism of restriction of intramolecular rotation (RIR).[5] It is noted that some novel AIE-active boron complexes bearing various ligands including ketoiminate,[6] diiminate,[7] pyridyl-enamido,[8] benzothiazole-enamide[9] and other heteroatom contained ligands[10] have been successfully developed.

Boranil, a kind of boron complex employing anil (also called salicylaldimine) as ligand, emerged as promising fluorescent materials in the field of bio-labelling and electroluminescent devices owing to their excellent optical properties as well as readily synthesis.[11] During the past years, great efforts have been put to increase the emission efficiency and extend the emission wavelength of boranil in solution state.[12] However, due to the lack of rational molecular design and modification, the strategy to construct the AIE-active boranil is still rare.[13]

Lipid droplets (LDs), the dynamic organelles for storage of neutral lipids, play crucial roles in many biological processes including lipid metabolism, membrane transport, protein degradation and signal transduction.[14,15] Abnormal lipid storage in LDs was reported to be associated with metabolic diseases such as fatty liver and cardiovascular diseases.[16] Therefore, development of high-performance fluorescent probes for imaging of LDs is of great importance for both biomedical research and early diagnosis of related diseases.

To address these issues, herein, we report a facile strategy to fabricate AIE-active boranil by installing phenyl ring as the intramolecular rotor in anil ligand (Scheme 1). **DEFB** is a well-known boranil complex and shows ACQ feature. Once two ethyl groups were replaced by phenyl rings, a new boranil complex (**DPFB**) was obtained, which displayed typical AIE effect. The solid-state emission of AIE-active boranil complexes were turned from 550 to 610 nm by introducing suitable substituents. Combining the theoretical calculation with single crystal analysis, distorted configuration and effective RIR in the condensed state should be responsible for the AIE characteristics of **DPFB** derivatives. Taking advantages of their good biocompatibility and suitable lipophilicity, **DPFB** derivatives could be successfully applied for imaging of LDs in living cells with fast and wash-free manners as well as staining of yolk lipids in zebrafish.

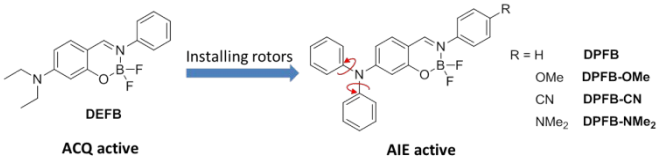

Scheme 1 Structures of **DEFB** and **DPFB** derivatives.

The synthetic routes of all boranil complexes were shown in Scheme S1. Anil ligands were easily prepared through the

[a] Key Laboratory of Macromolecular Science of Shaanxi Province, Key Laboratory of Applied Surface and Colloid Chemistry of Ministry of Education, Key Laboratory of the Ministry of Education for Medicinal Resources and Natural Pharmaceutical Chemistry, and School of Chemistry & Chemical Engineering, Shaanxi Normal University, Xi'an 710119, China. nzhao@snnu.edu.cn, nli@snnu.edu.cn.
†C.M. and W.Y. contributed equally to this work.
Electronic Supplementary Information (ESI) available: Synthesis and characterization, single crystal data, the absorption and emission spectra. See DOI: 10.1039/x0xx00000x

reaction of 4-(diethylamino)- or 4-(diphenylamino)-2-hydroxybenzaldehyde with corresponding aniline. Targeted complexes were obtained by treating anil with $BF_3{\cdot}Et_2O$ at basic condition. All complexes were fully characterized by NMR and high resolution mass spectrometry. In DMSO solution, both **DEFB** and **DPFB** exhibited strong π-π* transition at around 275 nm (Fig. S1A).[11] Meanwhile, remarkable absorption peaks at 400 nm were also observed, which could be attributed to the intramolecular charge transfer (ICT) transition. Upon photoexcition, **DEFB** emitted bright blue light (460 nm) with the quantum yield (Φ_f) of 4.0%. However, very faint emission centred at 550 nm (Φ_f = 0.7%) was obtained for **DPFB**. It is noteworthy that the Stokes shift of **DPFB** (150 nm) was significantly larger than **DEFB** (60 nm). Subsequently, the emission properties of **DEFB** and **DPFB** in the aggregated state were investigated. By adding the poor solvent of water into DMSO solution, the emission of **DEFB** was reduced gradually while the emission intensity at 460 nm dropped to 25% at water fraction (f_w) of 99% with Φ_f of 2.3% (Fig. 1A and 1B), suggesting its ACQ nature. In sharp contrast, with increasing of f_w (> 50%), the emission of **DPFB** was obviously enhanced (Fig. 1C and 1D). Approximately 300-fold enhancement at 567 nm was obtained when f_w reached 99% (Φ_f = 41.6%), indicative of its specific AIE effect. The molecular aggregation at f_w of 99% was confirmed by using dynamic light scattering measurement and the particle sizes were 469.5 and 119.3 nm for **DEFB** and **DPFB**, respectively (Fig. S2). In addition, the solid-state emission of **DEFB** and **DPFB** was detected at 495 nm (Φ_f = 2.1%) and 564 nm (Φ_f = 61.1%), respectively, which was consistent with their emission behaviour in aqueous solution (Fig. S1B).

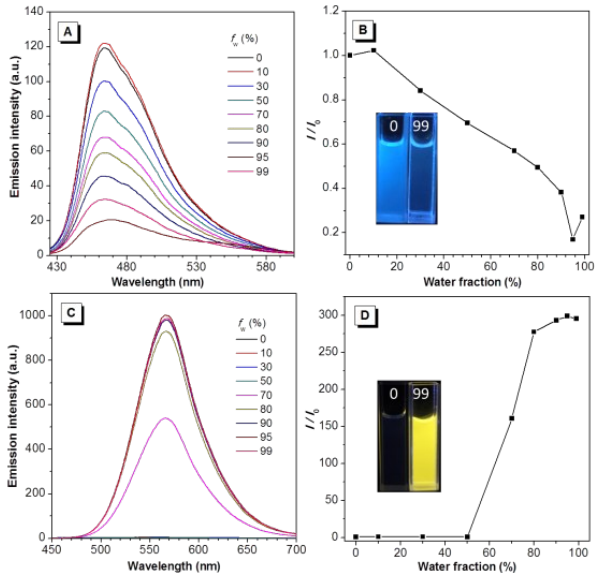

Fig. 1 Emission spectra of (A) **DEFB** and (C) **DPFB** in DMSO/water mixtures with varied f_w. Plot of I/I_0 of (B) **DEFB** and (D) **DPFB** versus f_w (I_0 represents the emission intensity in DMSO). Inset: photograph of (B) **DPFB** and (D) **DEFB** in DMSO/water mixtures with 0 and 99% f_w under 365 nm UV irradiation. λ_{ex}: 401 nm for **DEFB** and 403 nm for **DPFB**.

When different substituents including methoxyl, cyano and N,N-dimethyl groups were introduced into the para-position of aniline part, a series of boranil complexes (**DPFB-OMe**, **DPFB-CN** and **DPFB-NMe$_2$**) were obtained. All three complexes exhibited weak emission in solution, but gave intense emission in the aggregated state, indicative of their typical AIE effect (Fig. S3–S5). The solid-state emission of these **DPFB** derivatives was tuned from 495 to 601 nm (Fig. S1B). Meanwhile, **DPFB** derivatives exhibited high emission efficiency (Φ_f > 12.7%) after formed nano-aggregates in PBS solution (Fig. S1C and S6).

Table 1 The optical properties of **DEFB** and **DPFB** derivatives.

Complex	Solution[a]			Aggregation			
	λ_{abs} (nm)	λ_{em} (nm)	Φ_f[b] [%]	λ_{em}[c] (nm)	Φ_f[b] [%]	λ_{em}[d] (nm)	Φ_f[b] [%]
DEFB	401	460	4.0	460	2.3	461	1.9
DPFB	403	550	0.7	567	41.6	559	46.4
DPFB-OMe	408	535	1.0	550	18.2	556	20.1
DPFB-CN	419	530	0.5	573	16.5	574	16.0
DPFB-NMe$_2$	435	578	2.1	580	12.2	576	12.7

[a]In DMSO solution. [b]Absolute quantum yield determined by using a calibrated integrating sphere. [c]In DMSO/water (1/99) mixtures. [d]In DMSO/PBS (1/99) mixtures.

In order to investigate the different emission properties of **DEFB** and **DPFB** in solution state, optimized structures of two complexes in their ground (S_0) and excited (S_1) state were estimated using DFT and TD-DFT method, respectively. As shown in Fig. 2, the subtle difference for the structures of **DEFB** at S_0 and S_1 states was observed. Conversely, the molecular configuration of **DPFB** exhibited discrepancy from S_0 to S_1 state. This structure difference in **DPFB** implied the large structural relaxation in its S_1 state, which probably increased the ratio of non-radiative decay and resulted in the weak emission of **DPFB** in solution state.[17] For **DEFB**, non-radiative decay was effectively suppressed in the excited state due to its relative rigid structure. Thus, the bright emission observed for **DEFB** in solution state. Meanwhile, the large Stokes shift of **DPFB** could be ascribed to its large structural relaxation in the excited state.

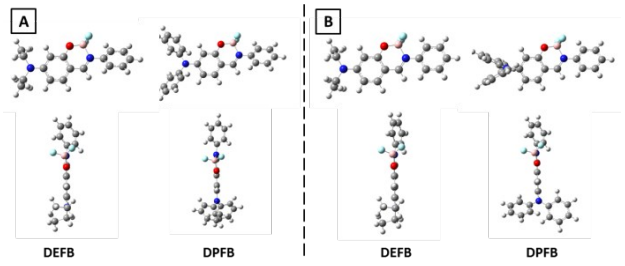

Fig. 2 Optimized structures of **DEFB** and **DPFB** in the (A) S_0 and (B) S_1 state.

The distribution and energy level of frontier orbits for **DPFB** derivatives were also calculated (Fig. S7). The highest occupied molecular orbital (HOMO) mainly located on the N,N-diphenyl groups and central part (phenyl ring and O-B-N chelate moiety), whereas the lowest unoccupied molecular orbital (LUMO) delocalized over the central part as well as aromatic group linked to the N atom of imine, which suggested the existence of ICT process in **DPFB** derivatives. The energy levels of HOMO were calculated to be -0.77 to -0.65 eV, and the energy levels of LUMO varied from -6.59 to -6.30 eV in the order from **DPFB**,

DPFB-OMe, **DFPB-CN** to **DFPB-NMe$_2$**. The corresponding energy gaps between HOMO and LUMO were 5.84, 5.82, 5.67 and 5.65 eV, which leaded to their red-shifted absorption behaviour (from 403 to 435 nm) in solution state.

Single crystals of **DEFB**, **DPFB-CN** and **DPFB-NMe$_2$** were obtained by slowly evaporating dichloromethane/*n*-hexane mixtures and characterized using single crystal X-ray diffraction (Table S1). As shown in Fig. 3, the aromatic ring linked to the imine was not coplanar with the core unit for all crystals and their torsion angles were measured as 42.02, 22.02 and 44.64^o for **DEFB**, **DPFB-CN** and **DPFB-NMe$_2$**, respectively. The additional torsion angles between two phenyl rings of N,N-diphenyl group and the central part were 73.45 (79.55) and 48.97 (55.07^o) for **DPFB-CN** and **DPFB-NMe$_2$**, respectively. Clearly, the replacement of ethyl group by phenyl ring in **DPFB** induced higher twisted configuration. Moreover, the dimer structures were formed in crystal of **DEFB** with a π-π stacking interaction (4.336 Å), which is considered as the primary cause for ACQ effect. However, the π-π stacking was avoided in crystal of **DPFB-CN** and **DPFB-NMe$_2$** due to their more distorted conformation. Meanwhile, weak interactions such as C–H···N (2.638, 2.617 Å) and C–H···F (2.453, 2.409 Å) were found in crystal of **DPFB-CN** and **DPFB-NMe$_2$**, which helped to rigidify their configuration (Fig. S8). In addition, the intramolecular rotation of **DPFB** derivatives was restricted once the molecules aggregated, which yielded the high emission efficiency.

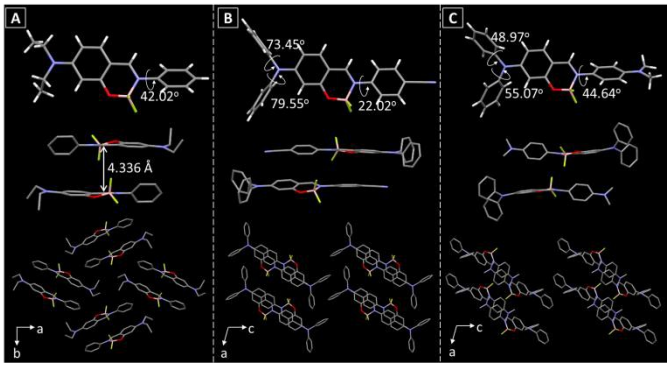

Fig. 3 Drawing of the crystal structure, side view and crystal packing of (A) **DEPB**, (B) **DPFB-CN** and (C) **DPFB-NMe$_2$**.

The excellent optical properties of **DPFB** derivatives inspired us to explore their bio-imaging applications. **DPFB** and **DPFB-NMe$_2$** were chosen for imaging experiments because of their distinct emission spectra. The biocompatibility was assessed using 4,5-dimethyl-2-thiazolyl)-2,5-diphenyltetrazolium bromide (MTT) assay (Fig. S9). When the concentration of **DPFB** derivatives reached up to 50 μM, cell viabilities were still more than 90%, demonstrated they possess low cytotoxicity. Then, the HeLa cells were incubated with **DPFB** derivatives and the pre-experiment results suggested that two complexes penetrated the cell membrane and accumulated in the LDs (Fig. S10). In order to further prove the intracellular localization of **DPFB** derivatives, the co-localization experiments were performed using commercial LDs marker (HCS LipidTOX™ Deep Red Neutral Lipid Stain). As illustrated in Fig. 4, the bright fluorescent signals from **DPFB** or **DPFB-NMe$_2$** channel were observed, which exactly overlapped with the signals derived from HCS LipidTOX™ Deep Red Neutral Lipid Stain. The overlap ratios were calculated to be 97 and 95% for **DPFB** and **DPFB-NMe$_2$**, implying that **DPFB** and **DPFB-NMe$_2$** can selectively stain the LDs in living cells. The suitable lipophilicities of **DPFB** derivatives with high ClogP value (6.24 for **DPFB** and 6.41 for **DPFB-NMe$_2$**) should be responsible for this specific LDs targeting.[18]

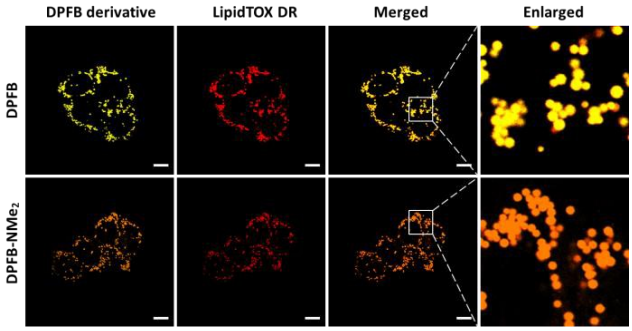

Fig. 4 Co-localization images of HeLa cells stained with **DPFB** derivatives (5 μM) and HCS LipidTOX™ Deep Red Neutral Lipid Stain (1:1000 dilution). Scale bar: 10 μm.

Owing to the unique AIE nature, we assessed the imaging capability of **DPFB** derivatives without washing step. After incubated cells with **DPFB** or **DPFB-NMe$_2$** for 30 min, the images were collected directly (Fig. 5A). It is interesting that the strong fluorescent signals from LDs with negligible background were observed, which is nearly no difference compared to the images after washing. However, the distinct background from cytoplasm was observed when the cells were treated with commercial probes BODIPY493/503 or Nile Red. This high signal-to-noise imaging with wash-free manner for **DPFB** derivatives could be attributed to the remarkable emission increase when molecules aggregated in LDs. This wash-free imaging mode will not only simplify the protocol for cell imaging, but also offer a convenient way to track the morphology of LDs in situ.

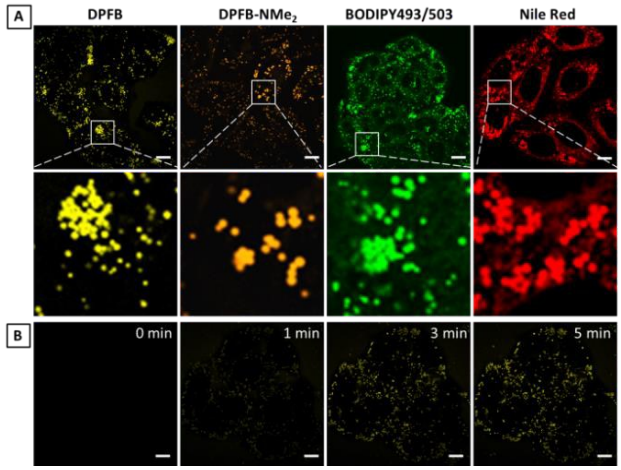

Fig. 5 (A) CLSM images of HeLa cells stained with **DPFB** derivatives (5 μM), BODIPY493/503 (500 nM) and Nile red (500 nM) without washing. (B) Time-dependent images of **DPFB** (5 μM). Scale bar: 10 μm.

The time-dependent staining of LDs using **DPFB** derivatives was studied. After added the **DPFB** derivatives into the cell culture medium, the images were collected with elapse of time. As described in Fig. 5B, yellow fluorescent signals started to appear when the incubated time was 1 min. After incubated cells to 3 min, the fluorescent signals became brighter and morphology of LDs was observed clearly. Similar short staining time (< 5 min) was obtained for **DPFB-NMe$_2$** (Fig. S11), indicated that **DPFB** derivatives can serve as ideal candidates for fast LDs staining.

In view of the selective LDs imaging of **DPFB** derivatives, their capability for imaging of living zebrafish was investigated because the zebrafish is an ideal model for studying the lipids related diseases.[19] Taking **DPFB-NMe$_2$** as example (Fig. 6), intense orange fluorescent signals originated from the yolk sac in zebrafish were observed after incubated with **DPFB-NMe$_2$** for 30 min. Similarly, yellow fluorescent signals in yolk sac were also obtained for **DPFB** (Fig. S12). Lots of neutral lipids and polar phospholipids exist in yolk, which provide energy for zebrafish at the initial stage of larval development. Therefore, above imaging results demonstrated that **DPFB** derivatives can stain the yolk lipids in zebrafish and has great potential for monitoring of lipids transport and metabolism processes.

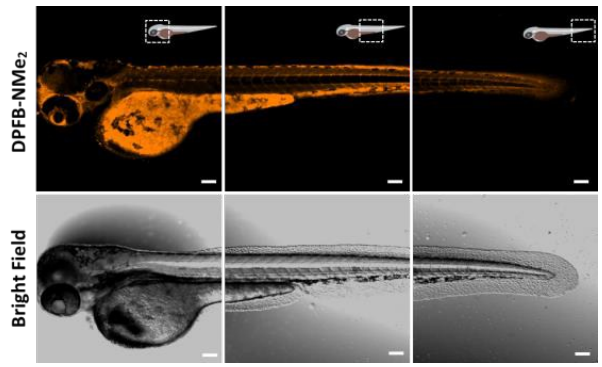

Fig. 6 CLSM images of zebrafish stained with **DPFB-NMe$_2$** (5 μM). Scale bar: 100 μm.

In summary, we reported a facile strategy to construct AIE-active boranil (**DPFB** derivatives) by installing phenyl ring as the intramolecular rotor within anil ligands. Based on the theoretical calculation and crystal analysis, the AIE nature of **DPFB** complexes was attributed to the distorted configuration as well as effective RIR in the aggregated state. In view of the good biocompatibility and suitable lipophilicity, **DPFB** and **DPFB-NMe$_2$** can selectively stain the LDs in living cells with fast and wash-free manners. Additionally, in vivo staining of yolk lipids in zebrafish was also successfully obtained. This work not only provides a convenient method to construct AIE-active boranil complex, but also extends their bio-imaging applications.

This work was supported by the National Natural Science Foundation of China (21672135, 51403122 and 21402115), the Fundamental Research Funds for the Central Universities (GK201902006 and GK201702002), Natural Science Foundation of Shaanxi Province (2018JM5086) and Funded Projects for the Academic Leaders and Academic Backbones, Shaanxi Normal University (18QNGG007).

Conflicts of interest

View Article Online
DOI: 10.1039/C9CC04041B

There are no conflicts of interest to declare.

Notes and references

1 (a) D. Li, H. Zhang and Y. Wang, *Chem. Soc. Rev.*, 2013, **42**, 8416−8433; (b) D. Frath, J. Massue, G. Ulrich and R. Ziessel, *Angew. Chem. Int. Ed.*, 2014, **53**, 2290−2310; (c) J. Wang, N. Wang, G. Wu, S. Wang and X. Li, *Angew. Chem. Int. Ed.*, 2019, **58**, 3082−3086.

2 (a) S. Kolemen and E. U. Akkaya, *Coord. Chem. Rev.*, 2018, **354**, 121−134; (b) T. Kowada, H. Maeda and K. Kikuchi, *Chem. Soc. Rev.*, 2015, **44**, 4953−4972.

3 (a) S. Choi, J. Bouffard and Y. Kim, *Chem. Sci.*, 2014, **7**, 751−755; (b) Q. Zhao and Z. Sun, *J. Mater. Chem. C.*, 2016, **4**, 10588−10609.

4 J. Luo, Z. Xie, J. W. Y. Lam, L. Cheng, H. Chen, C. Qiu, H. S. Kwok, X. Zhan, Y. Liu, D. Zhu and B. Z. Tang, *Chem. Commun.*, 2001, 1740−174.

5 (a) J. Mei, N. L. Leung, R. T. K. Kwok, J. W. Y. Lam and B. Z. Tang, *Chem. Rev.*, 2015, **115**, 11718−11940; (b) J. N. Zhang, H. Kang, N. Li, S. M. Zhou, H. M. Sun, S. W. Yin, N. Zhao and B. Z. Tang, *Chem. Sci.*, 2017, **8**, 577−582; (c) S. C. Hong, D. P. Murale, M. Lee, S. M. Lee, H. S. Park and J.-S. Lee, *Angew. Chem. Int. Ed.*, 2017, **56**, 14642–14647; (d) B. M. Chapin, P. Metola, S. L. Vankayala, H. L. Woodcock, T. J. Mooibroek, V. M. Lynch, J. D. Larkin and E. V. Anslyn, *J. Am. Chem. Soc.*, 2017, **139**, 5568–5578.

6 (a) R. Yoshii, A. Nagai, K. Tanaka and Y. Chujo, *Chem. Eur. J.*, 2013, **19**, 4506−4512; (b) H. S. Kumbhar and G. S. Shankarling, *Dyes and Pigments*, 2015, **122**, 85−93.

7 R. Yoshii, A. Hirose, K. Tanaka and Y. Chujo, *J. Am. Chem. Soc.*, 2014, **136**, 18131–18139.

8 X. Wang, Y. Du, Q. Liu, Z. Li, H. Yan, C. Ji, J. Duan and Z. Liu, *Chem. Commun.*, 2015, **51**, 784−787.

9 K. Li, J. Cui, Z. Yang, Y. Huo, W. Duan, S. Gong and Z. Liu, *Dalton Trans.*, 2018, **47**, 15002−15008.

10 (a) Y. Yang, X. Su, C. N. Carroll and I. Aprahamian, *Chem. Sci.*, 2012, **3**, 610−613; (b) J.-S. Ni, H. Liu, J. Liu, M. Jiang, Z. Zhao, Y. Chen, R. T. K. Kwok, J. W. Y. Lam, Q. Peng and B. Z. Tang, *Mater. Chem. Front.*, 2018, **2**, 1498−1570.

11 (a) D. Frath, S. Azizi, G. Ulrich, P. Retailleau and R. Ziessel, *Org. Lett.*, 2011, **13**, 3414−3417; (b) D. Frath, S. Azizi, G. Ulrich and R. Ziessel, *Org. Lett.*, 2012, **14**, 4774−4777.

12 (a) M. Urban, K. Durka, P. Jankowski, J. Serwatowski and S. Luliński, *J. Org. Chem.*, 2017, **82**, 8234−8241; (b) D. Frath, P. Didier, Y. Mély, J. Massue and G. Ulrich, *ChemPhotoChem*, 2017, **1**, 109−112.

13 S. Chen, R. Qiu, Q. Yu, X. Zhang, M. Wei and Z. Dai, *Tetrahedron Lett.*, 2018, **59**, 2671−2678.

14 M. Beller, K. Thiel, P. J. Thul and H. Jackle, *FEBS Lett.*, 2010, **584**, 2176−2182.

15 L. Tirinato, F. Pagliari, T. Limongi, M. Marini, A. Falqui, J. Seco, P. Candeloro, C. Liberale and E. Di Fabrizio, *Stem Cells Int.*, 2017, 1656053.

16 T. C. Walther and R. V. Farese, Jr., *Annu. Rev. Biochem.*, 2012, **81**, 687−714.

17 M. Yamaguchi, S. Ito, A. Hirose, K. Tanaka and Y. Chujo, *Mater. Chem. Front.*, 2017, **1**, 1573−1579.

18 M. Collot, T. K. Fam, P. Ashokkumar, O. Faklaris, T. Galli, L. Danglot and A. S. Klymchenko, *J. Am. Chem. Soc.*, 2018, **140**, 5401−5411.

19 X. Zheng, W. Zhu, F. Ni, H. Ai, S. Gong, X. Zhou, J. L. Sessler and C. Yang, *Chem. Sci.*, 2019, **10**, 2342−2348.

TOC: A series of boranil complexes with aggregation-induced emission effect were facile constructed, which can be utilized to image lipid droplets in living cells and yolk lipids in zebrafish.